International Journal of Natural and Engineering Sciences 9 (2): 51-57, 2015
ISSN: 1307-1149, E-ISSN: 2146-0086, www.nobel.gen.tr

Estimation of Aerodynamic Characteristics for a Horizontal Axis Wind Turbine

Akin ILHAN[1] Mehmet BILGILI[2] Besir SAHIN[1]* Huseyin AKILLI[1]
[1]Cukurova University, Faculty of Engineering and Architecture, Mechanical Engineering Department, Adana, Turkey
[2]Cukurova University, Ceyhan Engineering Faculty, Mechanical Engineering Department, Adana, Turkey

*Corresponding author:
Email: bsahin@cu.edu.tr

Received: May 20, 2015
Accepted: July 03, 2015

Abstract

Wind turbine aerodynamic characteristics play an important role in monitoring of condition and control of wind turbines in any wind power plant. Accurate estimation of these wind turbine aerodynamic characteristics is required to more realistic prediction of size of the storage capacity for wind energy integration. In this study, aerodynamic characteristics of horizontal axis wind turbine are modeled as a function of wind velocity (U_D) and atmospheric air temperature (T_{atm}) using artificial neural networks (ANNs). Wind velocity, U_D and atmospheric air temperature, T_{atm} are used as the input variables and wind power (P), power coefficient (C_P), axial flow induction factor (a), thrust coefficient (C_T) and thrust (T) are computed as the output layer. The measured values are compared versus those predicted by the ANN model and manufacture data. Results obtained from this study indicate that the ANN model can be a useful tool for accurate forecasting wind turbine aerodynamic characteristics. The most advantage of this model is that as long as having the required hub-height wind speed, U_D and atmospheric air temperature, T_{atm} wind turbine aerodynamic characteristics can be predicted without detailed knowledge of turbine operations and its control schemes.

Keywords: *Artificial neural network, turbine aerodynamic characteristics, wind power.*

INTRODUCTION

Without decisive action, energy related greenhouse gas emissions may become doubled by 2050, and increased oil demand will heighten concerns over the security of supplies. For this reason, an energy revolution is needed to achieve a 50% reduction of global CO_2 emissions relative to current levels by 2050. In this revolution, energy efficiency, sustainable and low-carbon energy technologies play a crucial role. In addition, renewable energy plays an important role in addressing global energy and environmental challenges [1]. Among renewable energy technologies, wind is the most advanced of the new renewable energy technologies. In a few countries, wind power already provides 15% to 30% of total electricity. The technology keeps rapidly improving, and costs of energy generation from the land-based wind installations have continued to fall. There is now 370 GW of installed wind power capacity in the world and a total of 128.8 GW is now installed in the European Union [2,3] as indicated in Figure 1.

As seen, wind energy has been developing towards a mainstream, competitive and reliable power technology. Globally, progress continues to be strong, with more active countries, ambitious manufacturers, increasing annual installment capacity and wide range of investments. According to the International Energy Agency [4] wind power could be generated up to 18% of the world's electricity by 2050, compared with 2.6% of today's capacity. Technology improvements have continuously reduced energy costs, especially on land. In this context, wind turbine aerodynamic characteristics estimation is an important tool in monitoring turbine performance, turbine control and power forecasting [5]. Because, effective integration of wind power into the power systems requires accurate estimation of the turbine power curve for operational management of wind energy as well as monitoring of turbine performance. Accurate estimation of wind turbine power characteristic curve is required to more realistically size the storage capacity for wind energy integration [5]. In this manner, an equivalent power characteristic curve for the entire plant can serve for the same purpose, for example, plant and system operators may use this curve to predict the plant output for a given wind speed [6].

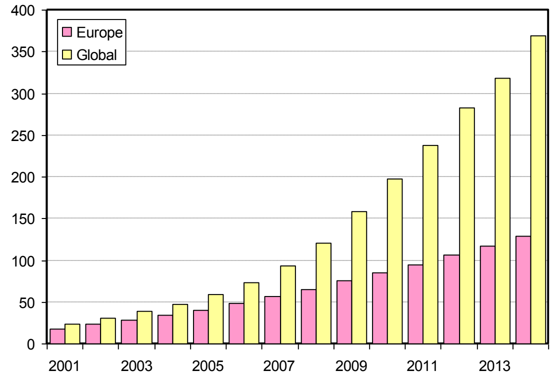

Figure 1. Development of wind power cumulative installed capacity in Europe and the world

The wind turbine capacity factor is an essential parameter in evaluating a wind turbine's efficiency [7]. In addition to this, the power characteristic curve is a wind turbine performance specification and an indicator of overall wind turbine health. Theoretical wind turbine power characteristic curves are obtained by manufacturers under assumption of ideal meteorological and topographical conditions. In practice, however, wind turbines are never used under ideal conditions, and the empirical wind turbine power characteristic curves could be substantially different from the theoretical ones due to the location of the turbine, air density, wind velocity distributions, wind directions, mechanical and control issues, as well as uncertainties in measurements [5]. In this context, the use of an equation for determining a power curve and the obtention of its parameters becomes an important issue [8]. Furthermore, accurate estimation of power characteristic curve serves as an important tool in wind power forecasting and aid in wind farm expansion [9, 10].

Today, the most common design of wind turbine is the horizontal axis wind turbine. In this study, horizontal axis wind turbine aerodynamic characteristics are modeled as a function of the hub-height wind speed. This turbine power curve and its aerodynamic characteristics model obtained for Belen Wind Farm in Turkey can be used for planning purposes and estimating total wind power production. The most advantage of this model is that as long as having the required hub-height wind speed, wind turbine aerodynamic characteristics can be predicted without detailed knowledge of turbine operations and its control schemes. Furthermore, they can also be predicted straightaway and satisfactorily without the use of other turbine characteristics, meteorological and topographical data.

MATERIAL AND METHODS

Study Region, Data and Turbine Technical Specifications

The data used in this study were measured from Belen Wind Power Plant (WPP). Belen WPP is in the Hatay, Turkey. The location of Belen WPP in Turkey is shown in Figure 2. This WWP is located on the geographical coordinates of $36^o12''$N $36^o28''$E latitude and longitude, respectively. It is located at an altitude of 474 m above sea level. It was put into operation in 2009. In the first phase, installed capacity of the plant is 30 MW. In 2010, the 6-MW capacity expansion provided with temporary admission, thus Belen WPP has reached 36 MW. Total installed capacity of Belen WPP has increased 48 MW with 4 extra turbines in 2012 and annual production amounts to about 150 million kWh. Belen WPP includes 16 identical wind turbines with the rated capacity of 3 MW, the hub height of 80 m and the rotor diameter of 90 m. A summary of the technical specifications for turbine is given in Table 1. The cut-in speed, rated speed, and cut-out speed of the turbines are 4 m/s, 15 m/s, and 25 m/s, respectively. Turbines of WPP are the VESTAS V90-3 MW wind turbine types. The VESTAS V90-3 MW wind turbine is a pitch regulated upwind turbine with active yaw and a three-blade rotor. The turbine utilizes the OptiTip and the variable speed concepts. With these features rated power will be maintained even in high wind speeds, regardless of air temperature and air density, and the wind turbine is able to operate the rotor at variable speed (RPM). At low wind speeds the OptiTip system and variable speed operation maximize the power output by giving the optimal RPM and pitch angle, which also minimizes the sound emission from the turbine.

Five wind turbines (T1, T2, T3, T4 and T5) were selected to evaluate the performance of the presented method. For each turbine, the collected data includes power output, P (kW), nacelle position (degree), wind speed, U_D from the anemometer on top of the nacelle (m/s) and atmospheric air temperature, T_{atm}. The existing hourly data cover a period of 1 year (2011). From this extensive dataset, the distributions of U_D, T_{atm} and P of all turbines are analyzed over a wide range of wind speeds.

Figure 2. The location of Belen WPP in Turkey

Table 1. Wind turbine technical properties

Equipment	Properties
Rotor	
Diameter	90 m
Area swept	6362 m^2
Nominal revolutions	16.1 rpm
Operational interval	8.6-18.4 rpm
Number of blades	3
Power regulation	Pitch/OptiSpeed
Air brake	Full blade pitch by three separate hydraulic pitch cylinders
Tower	
Hub height	80 m
Operational data	
Cut-in wind speed	4 m/s
Nominal wind speed	15 m/s
Cut-out wind speed	25 m/s
Generator	
Type	Asynchronous with OptiSpeed
Rated output	3000 kW
Operational data	50 Hz, 1000 V
Gearbox	
Type	Two planetary and one helical stage
Control	
Type	Microprocessor-based control of all the turbine functions with the option of remote monitoring. Output regulation and optimization via OptiSpeed and OptiTip pitch regulation

Aerodynamics of Horizontal Axis Wind Turbines

Figure 3 presents an energy extracting actuator disc and stream-tube. Practical horizontal axis wind turbine designs use airfoils to transform the kinetic energy of wind into useful energy. The analysis assumes a control volume, in which the control volume boundaries are the surface of a stream tube and two cross-sections of the stream tube. The turbine is represented by a uniform ‘actuator disc’ which creates a discontinuity of pressure in the stream tube of air flowing through it [11]. Note that this analysis is not limited to any particular type of wind turbine. The following assumptions are made for analysis:

- homogenous, incompressible, steady state fluid flow;

- no frictional drag;
- an infinite number of blades;
- uniform thrust over the disc or rotor area;
- a non–rotating wake;
- the static pressure far upstream and far downstream of the rotor is equal to the undisturbed ambient static pressure.

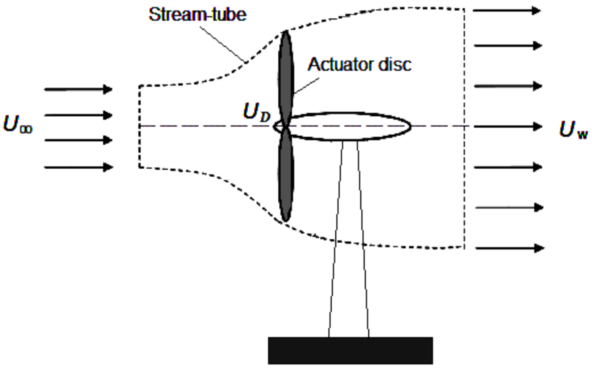

Figure 3. An energy extracting actuator disc and stream-tube

Figure 3 shows an energy extracting actuator disc and stream-tube. The disc upstream of the stream-tube has a cross-sectional area smaller than that of the disc and an area larger than the disc downstream. The conservation of mass principle for steady flow can be expressed as;

$$\dot{m}_{in} = \dot{m}_{out} \tag{1}$$

$$\rho A_\infty U_\infty = \rho A_D U_D = \rho A_W U_W \tag{2}$$

Where ρ is the air density, A is the cross-sectional area and U is the flow velocity. The symbol ∞ refers to conditions far upstream, D refers to conditions at the disc and W refers to conditions in the far wake. The actuator disc induces a velocity variation which must be superimposed on the free stream velocity, and so the net stream-wise velocity is [11]:

$$U_D = U_\infty (1-a) \tag{3}$$

and

$$U_W = U_\infty (1-2a) \tag{4}$$

Where a is called the axial flow induction factor, or inflow factor. The thrust force, T on the air and the power extraction, P from the air are calculated by;

$$T = 2\rho A_D U_\infty^2 a(1-a) \tag{5}$$

$$P = 2\rho A_D U_\infty^3 a(1-a)^2 \tag{6}$$

A power coefficient is defined as:

$$C_p = \frac{P}{\frac{1}{2}\rho U_\infty^3 A_D} \tag{7}$$

or,

$$C_p = 4a(1-a)^2 \tag{8}$$

The maximum value of C_p occurs when

$$\frac{dC_p}{da} = 4(1-a)(1-3a) = 0 \tag{9}$$

that gives a value of a=1/3. Hence,

$$C_{p_{\max}} = 16/27 = 0.593 \tag{10}$$

The maximum achievable value of the power coefficient is known as the Betz limit [11]. The force on the actuator disc caused by the pressure drop can also be non-dimensionalised to provide a thrust coefficient, C_T,

$$C_T = \frac{T}{\frac{1}{2}\rho U_\infty^2 A_D} \tag{11}$$

$$C_T = 4a(1-a) \tag{12}$$

Artificial neural networks

Artificial neural networks are computational networks which attempt to simulate, in a gross manner, the networks of nerve cell of the biological central nervous system. The neural network is in fact a novel computer architecture and a novel algorithmization architecture relative to conventional computers. It allows using very simple computational operations to solve complex, mathematically ill-defined problems, nonlinear problems or stochastic problems [12,13].

The main contribution of ANNs is that it allows for very low level programming to allow solving complex problems, especially those that are non-analytical and/or nonlinear and/or nonstationary and/or stochastic, and to do so in a self-organizing manner that applies to a wide range of problems with no re-programming or other interference in the program itself [14,15].

In the literature, there are many types of ANN such as Feed Forward Neural Networks (FFNN), Radial Basis Neural Networks (RBNN) and Generalized Regression Neural Networks (GRNN). The learning of ANNs is generally accomplished by a back-propagation algorithm. Back-propagation (BP) is the most commonly used supervised training algorithm in multilayered FFNNs. In back-propagation networks, information is processed in the forward direction from the input layer to the hidden layer and then to the output layer. The objective of a back-propagation network is to find the optimal weights which will generate an output vector as close as possible to the target values of the output vector with a selected accuracy by minimizing a predetermined error function [12-15].

The fundamental processing element of a neural network is a neuron. The BP algorithm starts, of necessity with computing the output layer, which is the only one where desired outputs are available, but the outputs of the intermediate layers are unavailable (Figure 4), as follows [16]:

Error-energy at the output layer is shown by ε in order to define,

$$\varepsilon = \frac{1}{2}\sum_k (d_k - y_k)^2 = \frac{1}{2}\sum_k e_k^2 \tag{13}$$

The term “k” of the summation formula includes the subsequent numbers starting from 1 to N, where N is the number of neurons in the output layer. Consequently, the gradient on the ε is considered, where:

$$\nabla\varepsilon_k = \frac{\partial\varepsilon}{\partial w_{kj}} \qquad (14)$$

Here, with the consideration of steepest gradient procedure, we have

$$w_{kj}(m+1) = w_{kj}(m) + \Delta w_{kj}(m) \qquad (15)$$

The j^{th} input to the output layer of the neuron involving in the series with the order of k^{th}, where, with the steepest descent procedure again, Δw_{kj} is defined in equation 16 below.

$$\Delta w_{kj} = -\eta\frac{\partial\varepsilon}{\partial w_{kj}} \qquad (16)$$

The k's perceptron's node-output z_k is defined with the multiplication of “w_{kj}” and “x_j” terms in the sigma formula as presented in equation 17.

$$z_k = \sum_j w_{kj}x_j \qquad (17)$$

The j^{th} input to that neuron is x_j, and the perceptron’s output is y_k where a nonlinear function defines this output:

$$y_k = F_N(z_k) \qquad (18)$$

F is the nonlinear function. We can now substitute,

$$\frac{\partial\varepsilon}{\partial w_{kj}} = \frac{\partial\varepsilon}{\partial z_k}\frac{\partial z_k}{\partial w_{kj}} \qquad (19)$$

And,

$$\frac{\partial z_k}{\partial w_{kj}} = x_j(p) = y_j(p-1) \qquad (20)$$

$$\frac{\partial\varepsilon}{\partial w_{kj}} = \frac{\partial\varepsilon}{\partial z_k}x_j(p) = \frac{\partial\varepsilon}{\partial z_k}y_j(p-1) \qquad (21)$$

The output layer is p. Defining:

$$\Phi_k(p) = -\frac{\partial\varepsilon}{\partial z_k(p)} \qquad (22)$$

$$\frac{\partial\varepsilon}{\partial w_{kj}} = -\Phi_k(p)x_j(p) = -\Phi_k y_j(p-1) \qquad (23)$$

$$\Delta w_{kj} = \eta\Phi_k(p)x_j(p) = \eta\Phi_k(p)y_j(p-1) \qquad (24)$$

J shows the jth input to neuron k of the output (p) layer. In addition,

$$\Phi_k = -\frac{\partial\varepsilon}{\partial z_k} = -\frac{\partial\varepsilon}{\partial y_k}\frac{\partial y_k}{\partial z_k} \qquad (25)$$

$$\frac{\partial\varepsilon}{\partial y_k} = -(d_k - y_k) = y_k - d_k \qquad (26)$$

and, for a sigmoid nonlinearity:

$$y_k = F_N(z_k) = \frac{1}{1+\exp(-z_k)} \qquad (27)$$

$$\frac{\partial y_k}{\partial z_k} = y_k(1-y_k) \qquad (28)$$

Consequently, with the consideration of equations (25), (26) and (28), Φ_k is given with the equation 29.

$$\Phi_k = y_k(1-y_k)(d_k - y_k) \qquad (29)$$

At the output layer, following expressions are written:

$$\Delta w_{kj} = -\eta\frac{\partial\varepsilon}{\partial w_{kj}} = -\eta\frac{\partial\varepsilon}{\partial z_k}\frac{\partial z_k}{\partial w_{kj}} \qquad (30)$$

$$\Delta w_{kj}(p) = \eta\Phi_k(p)y_j(p-1) \qquad (31)$$

In Eq. (29), Φ_k was given in order to complete the derivation of the setting of output layer weights.

If we propagate back for the hidden layer of rth order with the consideration of ith branch into the neuron of jth order, we again have the same as before, and consequently in parallel to Eq. (19), we can constitute equations 32 and 33.

$$\Delta w_{ji} = -\eta\frac{\partial\varepsilon}{\partial w_{ji}} \qquad (32)$$

$$\Delta w_{ji} = -\eta\frac{\partial\varepsilon}{\partial z_j}\frac{\partial z_j}{\partial w_{ji}} \qquad (33)$$

When Eq. (20) is noted and the definition of Φ in Eq. (25) is defined, equation 34 can be set up as follows:

$$\Delta w_{ji} = -\eta\frac{\partial\varepsilon}{\partial zj}y_i(r-1) = \eta\Phi_j(r)y_i(r-1) \qquad (34)$$

When the right hand-side relation of Eq. (25) is considered, definition of equation (35) can be obtained:

$$\Delta w_{ji} = -\eta\left[\frac{\partial\varepsilon}{\partial y_j(r)}\frac{\partial y_j}{\partial z_j}\right]y_i(r-1) \qquad (35)$$

Here, $\partial\varepsilon/\partial y_j$ is inaccessible. Finally, $\Phi_j(r)$ can be given as:

$$\Phi_j(r) = y_j(r)\left[1-y_j(r)\right]\sum_k \Phi_k(r+1)w_{kj}(r+1) \qquad (36)$$

The mean absolute percentage error (MAPE) and correlation coefficient (R) were used to see the convergence between the target values and the output values. Here, MAPE is defined as follows:

$$MAPE = \frac{1}{n}\sum_{i=1}^{n}\frac{\left|p_i - m_i\right|}{p_i}x100 \qquad (37)$$

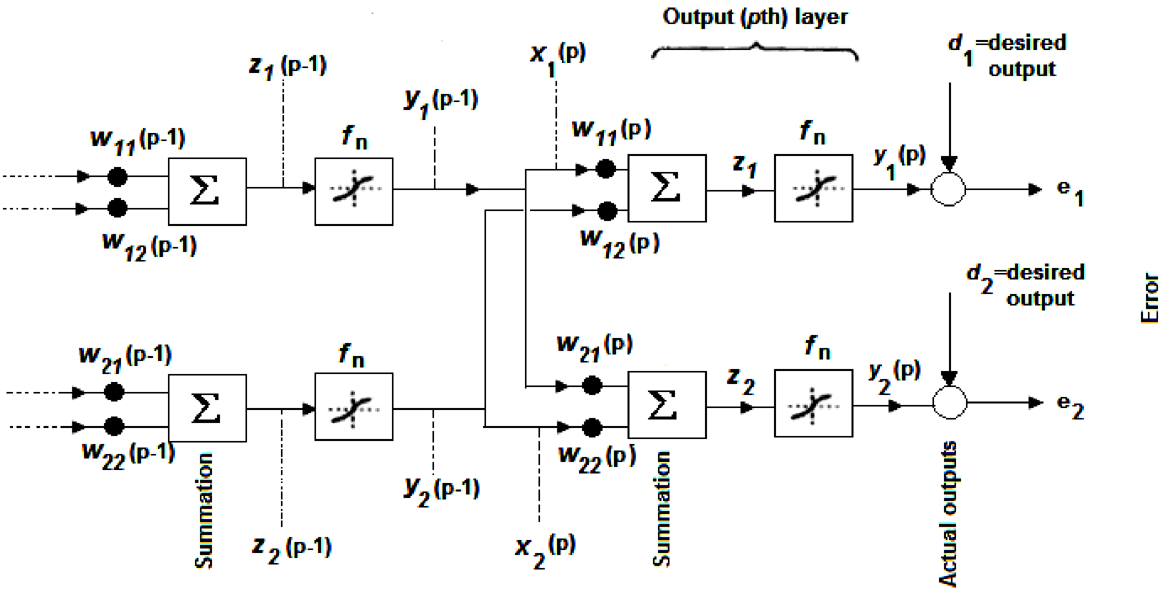

Figure 4. A multi-layer perceptron

RESULTS AND DISCUSSION

For the development of forecasting models, the hourly data records were collected in the period of 2011 for five turbines (T1, T2, T3, T4 and T5). Some turbine aerodynamic characteristic data including missing values were removed from the data set. From the extensive data set, distributions of U_D, T_{atm} and P of all turbines were analyzed over a wide range of wind speeds. Other turbine aerodynamic characteristics such as C_P, a, C_T and T were calculated using U_D and P parameters. First, the total 288 data records were divided into two subsets such as training and testing data set. The training data set includes 236 data covered the turbines of T1, T3, T4 and T5 which are approximately 80% of the total data. The testing data set covered the turbine of T2 consists of 62 data which are 20% of the total data. So, turbine aerodynamic characteristics (P, C_P, a, C_T and T) can be characterized as the function of U_D and T_{atm}. The relationship between the turbine aerodynamic characteristics and independent variables can be expressed as:

$$\left(P,a,C_p,C_T,T\right)=f\left(U_D,T_{atm}\right)$$

The selected independent variables determine the structure of forecasting model and affect the results of the model and the weighted coefficient. For this reason, the selection of the most suitable independent variables is very important tool in the forming of satisfactory forecasting model. The ANN architecture used in this study is shown in Figure 5. As seen in this figure, wind velocity, U_D and atmospheric air temperature, T_{atm} were used as input variables. Two different input combinations (Model 1 and Model 2) were used for estimating wind power (P), power coefficient (C_P), axial flow induction factor (a), thrust coefficient (C_T) and thrust (T). In Model 1, there is one input parameter into the network, which consisted of U_D. On the other hand, there are two input parameters (U_D and T_{atm}) for Model 2. The parameters of U_D and T_{atm} are the most important climatic factors influencing performance of turbine aerodynamic characteristics. These parameters are more readily available in this region and all over the word. Moreover, they can be measured and obtained easily in any regions of the world.

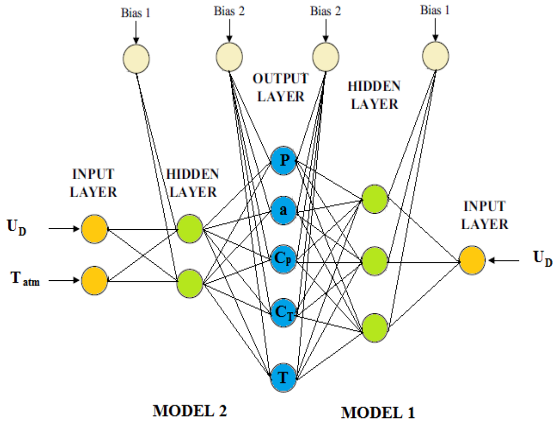

Figure 5. ANN architecture used in this study

In order to determine the optimal network architecture, various structures of forecasting models were designed under MATLAB software. For this reason, the predictions were performed by taking different number of hidden layer neurons between 1 and 10. Models 1 and 2 were tested by testing data set, which was not used during the training process. Different training algorithms were used, and the best fit result was obtained. In these models, Levenberg–Marquardt (LM) learning algorithm was used. Neurons in the input layer have no transfer function. Logistic sigmoid transfer function (logsig) and linear transfer function (purelin) were applied in the hidden layers and output layer of the network as an activation function, respectively. The ANN architecture consists of an input layer, an output layer and one hidden layer with three and two neurons for Models 1 and 2, respectively. In the training procedure, the maximum epoch’s number was set to 300, and the mean square error goal was set to 5×10^{-5}.

Models 1 and 2 were trained and tested to compare and evaluate the performances of ANNs. The input combinations and obtained equations of ANN models are given in Table 2. These equations can be used for the

Table 2. The input combinations and obtained equations of ANN models

Output	Input	Model	Equation
P	U_D	Model 1	$P=\frac{1511.118}{1+e^{-949.732U_D-98.65}}-\frac{3209.861}{1+e^{0.427U_D-4.266}}-\frac{48.206}{1+e^{-3122.747U_D+1394.805}}+1588.875$
	U_D and T_{atm}	Model 2	$P=\frac{3210.86}{1+e^{-0.416U_D-0.025T_{atm}+4.627}}-\frac{867.528}{1+e^{-708.578U_D-611.768T_{atm}+236.175}}+746.762$
a	U_D	Model 1	$a=\frac{0.079}{1+e^{-0.008U_D+20.64}}-\frac{0.078}{1+e^{0.434U_D-6.028}}-\frac{24.019}{1+e^{-1.464U_D-0.835}}-23.998$
	U_D and T_{atm}	Model 2	$a=\frac{17.106}{1+e^{-0.199U_D-0.0004T_{atm}-2.62}}-\frac{8.915}{1+e^{-0.16U_D+0.007T_{atm}-2.026}}-8.194$
C_p	U_D	Model 1	$C_P=-\frac{0.074}{1+e^{-0.947U_D+11.345}}+\frac{0.173}{1+e^{0.475U_D-7.817}}+\frac{11.082}{1+e^{-2.214U_D+3.95}}-10.943$
	U_D and T_{atm}	Model 2	$C_P=\frac{3.804}{1+e^{0.126U_D-0.001T_{atm}+0.474}}-\frac{6.605}{1+e^{0.186U_D+0.015T_{atm}+1.162}}-0.047$
C_T	U_D	Model 1	$C_T=-\frac{0.19}{1+e^{-0.477U_D+7.771}}+\frac{0.088}{1+e^{0.963U_D-11.441}}+\frac{8.677}{1+e^{-2.187U_D+4.276}}-8.421$
	U_D and T_{atm}	Model 2	$C_T=-\frac{0.703}{1+e^{-0.196U_D+0.003T_{atm}+1.945}}+\frac{0.957}{1+e^{-0.249U_D-0.067T_{atm}+0.793}}-0.239$
T	U_D	Model 1	$T=-\frac{139.356}{1+e^{35.882U_D+96.786}}+\frac{175.726}{1+e^{0.227U_D-3.645}}+\frac{288.232}{1+e^{0.403U_D+3.318}}-187.64$
	U_D and T_{atm}	Model 2	$T=\frac{130.309}{1+e^{0.355U_D+0.022T_{atm}-6.443}}+\frac{264.079}{1+e^{-0.339U_D-0.054T_{atm}+3.692}}-146.342$

Table 3. The training and testing results of Models 1 and 2

Characteristics	**Training procedure**				**Testing procedure**			
	MAPE (%)		**R**		**MAPE (%)**		**R**	
	Model 1	**Model 2**	**Model 1**	**Model 2**	**Model 1**	**Model 2**	**Model 1**	**Model 2**
P	4.88	4.63	0.9965	0.9967	3.71	3.54	0.9995	0.9991
a	4.82	4.61	0.9787	0.9811	3.86	3.84	0.9977	0.9950
C_p	3.73	3.67	0.9839	0.9842	2.62	2.82	0.9987	0.9959
C_T	4.13	4.07	0.9818	0.9820	2.93	3.15	0.9986	0.9950
T	5.12	4.71	0.9896	0.9909	3.85	3.43	0.9983	0.9972

prediction of aerodynamic characteristics of the VESTAS V90-3 MW wind turbines. The training and testing results of Models 1 and 2 are given in Table 3. Comparing the results of these models, it is seen that the performance values of Model 2 are generally better than Model 1. According to the derived results, based on the testing data set, the MAPE and R ranged from 2.62% to 3.86% and 0.9950–0.9995, respectively. These results indicate that artificial intelligence models can be a useful tool for accurate forecasting wind turbine aerodynamic characteristics based on wind speed, U_D and atmospheric air temperature T_{atm}. The scatter diagrams of the network predictions against the actual values and manufacture curves were drawn in order to indicate the performance of the ANN models. As seen in Figures 6-10, the results of prediction have fairly close agreement with the corresponding actual values.

CONCLUSIONS

The main objective of this study is to develop ANN models for estimating wind turbine aerodynamic characteristics, so that the wind plant performance can be characterized with a few measured or predicted input variables such as wind speeds, U_D and atmospheric air temperatures, T_{atm}. Equivalent wind plant aerodynamic characteristic curves obtained in the present study become highly desirable and useful in predicting plant output for a given wind forecast. According to the derived results, based on the testing data set, the MAPE and R ranged from 2.62% to 3.86% and 0.9950–0.9995, respectively. These results indicate that artificial intelligence models can be a useful tool for accurate forecasting wind turbine aerodynamic characteristics based on wind speed, U_D and atmospheric air temperature, T_{atm}. The most advantage of this model is that as long as having the required hub-height wind speed, U_D and atmospheric air temperature, T_{atm} wind turbine aerodynamic characteristics can be predicted without detailed knowledge of turbine operations and its control schemes.

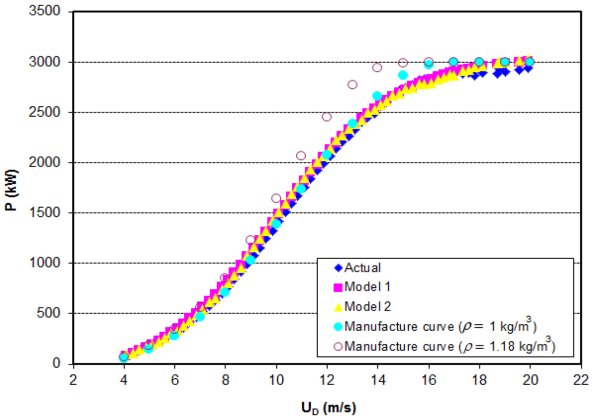

Figure 6. Comparison between prediction and actual results for *P*

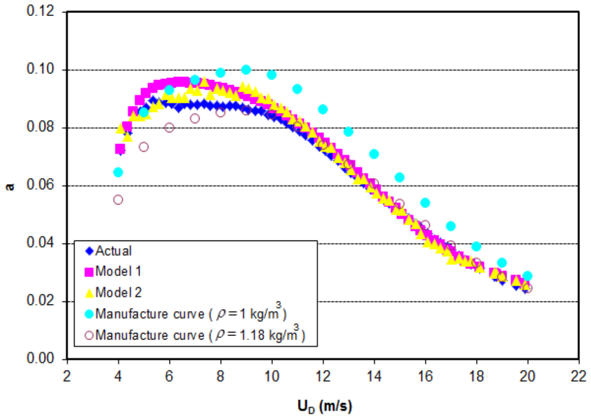

Figure 7. Comparison between prediction and actual results for *a*

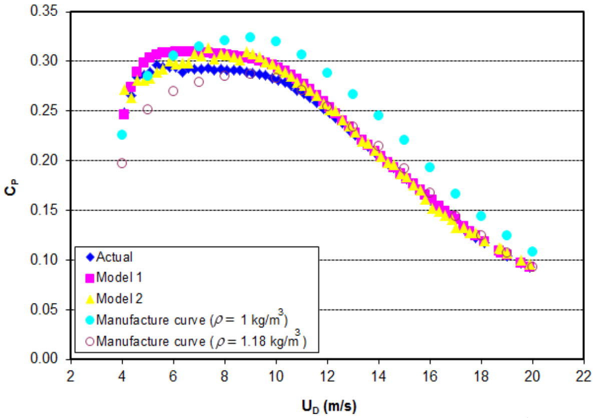

Figure 8. Comparison between prediction and actual results for C_P

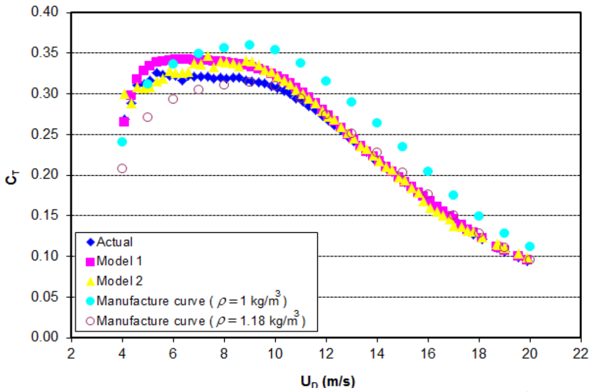

Figure 9. Comparison between prediction and actual results for C_T

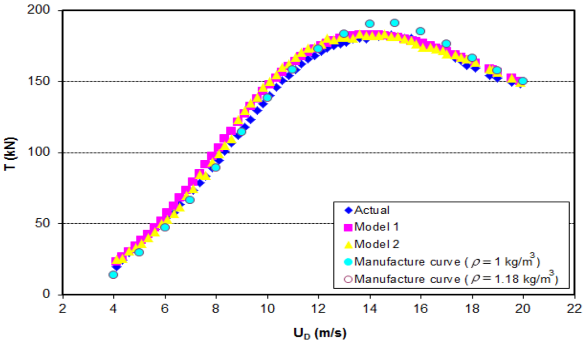

Figure 10. Comparison between prediction and actual results for *T*

REFERENCES

[1] Bilgili M, Ozbek A, Sahin B and Kahraman A. 2015. An overview of renewable electric power capacity and progress in new technologies in the world. Renewable and Sustainable Energy Reviews. 49:323-334.

[2] GWEC, Global Wind Energy Council, Global wind report. 2015. http://www.gwec.net.

[3] EWEA, European Wind Energy Association, Wind in power 2014 European Statistics, 2015, http://www.ewea.org.

[4] IEA, International Energy Agency, Energy Statistics Manual, 2013, https://www.iea.org.

[5] Shokrzadeh S, Jozani MJ and Bibeau E. 2014. Wind turbine power curve modeling using advanced parametric and nonparametric methods. IEEE Transactions on Sustainable Energy. 5:1263-1269.

[6] Wan YH, Ela E and Orwig K. Development of an equivalent wind plant power-curve. National Renewable Energy Laboratory. Dallas, Texas, May 23-26, 2010.

[7] Chang TP, Liu FJ, Ko HH, Cheng SP, Sun LC and Kuo SC. 2014. Comparative analysis on power curve models of wind turbine generator in estimating capacity factor. Energy. 73:88-95.

[8] Carrillo C, Montano AFO and Diaz-Dorado JCE. 2013. Review of power curve modelling for wind turbines. Renewable and Sustainable Energy Reviews. 21:572-581.

[9] Lydia M, Kumar SS, Selvakumar AI and Kumar GEP. 2014. A comprehensive review on wind turbine power curve modeling techniques. Renewable and Sustainable Energy Reviews. 30:452-460.

[10] Trivellato F, Battisti L and Miori G. 2012. The ideal power curve of small wind turbines from field data. J. Wind Eng. Ind. Aerodyn. 108:263-273.

[11] Burton T, Sharpe D, Jenkins N and Bossanyi E. 2001. Wind energy handbook. John Wiley & Sons, LTD, England.

[12] Bilgili M. 2010. Prediction of soil temperature using regression and artificial neural network models. Meteorol Atmos Phys.110:59-70.

[13] Bilgili M and Ozgoren M. 2011. Daily total global solar radiation modeling from several meteorological data. Meteorol Atmos Phys. 112:125-138.

[14] Cobaner M, Citakoglu H, Kisi O and Haktanir T. 2014. Estimation of mean monthly air temperatures in Turkey. Computers and Electronics in Agriculture.109:71-79.

[15] Ay M and Kisi O. 2014. Modelling of chemical oxygen demand by using ANNs, ANFIS and k-means clustering techniques. Journal of Hydrology. 511:279-289.

[16] Graupe D. 2007. Principles of artificial neural networks, 2nd Edition. World Scientific Publishing Co. Pte. Ltd. USA.